

Wear-Resistant Cast Iron Containing Spheroidal Graphite with a Two-Layer Ledeburitic–Martensitic Shell

L. V. Kostyleva^{a, *}, D. S. Gapich^a, A. E. Novikov^{b, c, **}, and V. A. Motorin^{a, c}

^aVolgograd State Agrarian University, Volgograd, Russia

^bVolgograd State Technical University, Volgograd, Russia

^cAll-Russia Research Institute of Irrigated Agriculture, Volgograd, Russia

*e-mail: kostyleva.l.v@yandex.ru

**e-mail: novikov-ae@mail.ru

Received July 24, 2018; revised December 26, 2018; accepted January 21, 2019

Abstract—The structure of a precipitation-hardened composite material, which consists of hard graphite inclusions coated with a two-layer ledeburite–martensite shell and uniformly distributed in a ductile metallic base, forms in the transition layer of high-strength spheroidal graphite cast iron chilled by surface quenching with melting. A process of volume heat treatment is proposed to form this structure in the volume of a product and to increase the abrasive wear resistance, the strength, and the impact toughness.

Keywords: high-strength spheroidal graphite cast iron, volume heat treatment, structure of precipitation-hardened composite material, abrasive wear resistance, strength, impact toughness

DOI: 10.1134/S0036029520030064

INTRODUCTION

The materials of machine components that operate under the severe conditions of abrasive wear, high contact pressures, and significant impact actions must have high wear resistance, high strength characteristics, and high impact toughness [1, 2]. As follows from Charpy's principle, this set of properties can be ensured by heterophase matrix microstructures, which should consist of isolated hard particles uniformly distributed in a continuous and high-strength matrix. A similar principle of structure formation is used in modern technologies of production of precipitation-hardened composites.

During operation, solid particles in a structure undergo the maximum contact loads and withstand the shear action of abrasive grains from the environment. A continuous matrix holds these particles in a material and serves for the redistribution and averaging of an external load and for the decreasing and relaxation of appearing stresses. In addition, microplastic deformation, which hinders the brittle fracture of a contact layer, develops in this matrix.

Cast iron is a promising material for producing articles with high tribotechnical and strength characteristics [3, 4]. Changing the chemical composition and the cooling rate during solidification or heat treatment, researchers can form a wide spectrum of structures, which have a wide variety of phase compositions, sizes, and morphologies of structural constitu-

ents, meet Charpy's principle, and have high wear resistance and impact toughness.

White cast iron, which contains high contents of chromium, molybdenum, other carbide-forming elements, nickel, and copper, has the maximum wear resistance. However, white chromium–nickel cast iron ingots cannot be machined and are susceptible to brittle fracture. Therefore, in spite of a high hardness and abrasive wear resistance, white cast iron is rarely used in mechanical engineering. The high-hardness carbide phase in the microstructure of white cast iron forms a continuous skeleton throughout a bainitic or martensitic–austenitic metallic base. However, according to Charpy's principle, complete inversion of hard inclusions in a ductile matrix is required (i.e., hard particles should be isolated from each other).

A eutectic has signs of inversion in the form of acicular carbides, which are uniformly distributed from the center of a eutectic colony in a continuous austenitic matrix in vanadium white cast iron [5]. The wear resistance of vanadium cast iron with an inverted eutectic approaches that of high-speed steel and can be machined with a hard-alloy cutting tool at a strength $\sigma_u \leq 1000$ MPa, plasticity $\delta \leq 2.5\%$, and a hardness HB 388. However, the high cost of the alloying elements, an insufficient impact toughness, and some technological difficulties restrict a wide application of vanadium white cast iron in, e.g., agriculture, road building, and mining.

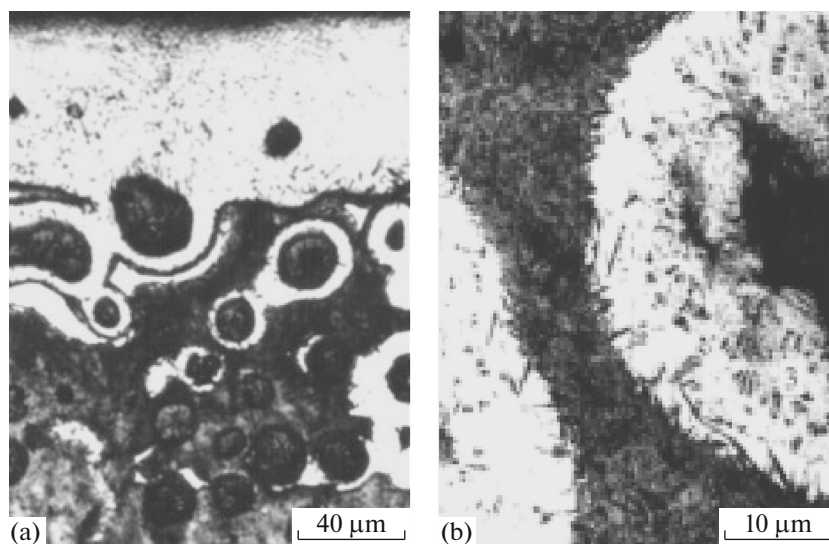


Fig. 1. Micrographs ((a) $\times 250$, (b) $\times 1400$) of the transition layer in spheroidal graphite cast iron after LHT with surface melting.

The structure formation in plain graphitized and partly chilled cast iron usually does not correspond to Charpy's principle, since eutectic cementite in it forms along austenite–graphite cell boundaries and creates layers in the form of a spatial continuous or partly discontinuous network.

At present, many Russian and foreign researchers [6–10] propose to use high-strength cast iron with spheroidal graphite and eutectic cementite to produce wear-resistant machine components. This cast iron was called carbidic austempered ductile iron (CADI). In essence, CADI is high-strength spheroidal graphite cast iron, the structure of which contains 10–30 vol % cementite and can be formed during eutectic solidification due to alloying and supercooling. The microstructure of a metallic base is formed by isothermal quenching and can be bainitic, ausferritic,¹ or martensitic–ferritic depending on the properties to be achieved. CADI castings operate well under abrasive wear and are inferior to graphitized bainitic cast iron with spheroidal graphite in viscoplastic characteristics and machining. The main causes of these disadvantages are the large sizes and unfavorable morphology of cementite inclusions, which have sharp edges and an acute-angled shape. In addition, when the number of these inclusions is large, they form a network along eutectic cell boundaries and promote brittle dislodging of eutectic cells under high contact pressures.

A combination of wear resistance and a high strength with a high impact toughness is achieved in spheroidal graphite cast iron castings with a “hard eye structure” [11, 12]. This structure mainly consists of a ferrite matrix and spheroidal graphite inclusions,

¹ Bainitic structure consisting of acicular ferrite and austenite.

around which bainite or martensite microshells form during heat treatment.

The mechanism of the influence of the hard eye structure on the impact toughness of cast iron consists in the fact that the hard bainite or martensite shell at the graphite/matrix interface has a high strength and hardness and, hence, substantially hinders its fracture, increasing the crack nucleation energy.

The phase composition and the size and morphological characteristics of the hard eye structure in high-strength spheroidal graphite cast iron (HSSGCI) make it possible to attribute it to the category of precipitation-hardened particle-reinforced composites according to Frommeyer's classification [13].

The reinforcing action of particles in the hard eye structure increases with the hardness of the shells surrounding spheroidal graphite.

The metallographic studies [14, 15] of HSSGCI hardened by laser heat treatment (LHT) with surface melting revealed a thin layer in the transition zone, which has well-pronounced signs of the hard eye structure. Specifically, graphite globules coated with a hard ledeburite shell are uniformly distributed in a martensitic–austenitic metallic matrix (Fig. 1).

The formation of ledeburite shells around graphite inclusions during LHT was assumed to be related to intense laser radiation absorption by graphite particles and to a decrease in the melting temperature of the neighboring carbon-rich metal regions [15]. As a result, a thin contact metal layer at the graphite/metallic base interface undergoes contact melting, and a metastable eutectic (ledeburite) forms in this layer upon solidification at a large supercooling.

Contact melting, which was first described by Saratovkin, manifests itself as the solid–liquid phase transition in eutectic systems in the zone of contact of

Table 1. Chemical composition and mechanical properties of experimental VCh50 cast iron

Element content, wt %						Mechanical properties			
C	Mn	Si	S	P	Mg	σ_u	σ_y	$\delta, \%$	<i>HB</i>
						MPa			
3.39	0.51	2.71	0.041	0.100	0.04	613	446	5.0	268

Table 2. HT schedules for VCh50 cast iron (1, schedule for standard (grade 45 steel); 2–6, schedules for cast iron)

HT schedule	HT conditions
1	Normalizing at 880°C
2	Surface laser quenching: track overlapping of 30%, power $P = 2$ kW, beam speed $v = 480$ mm/min, beam diameter $d = 9$ mm
3	RF current surface quenching: power $P = 180$ kW, frequency $\nu = 45$ kHz
4	Volume isothermal quenching: heating in salt bath to $t = 950^\circ\text{C}$, holding for $\tau = 2$ h, transfer to bath with $t = 380^\circ\text{C}$, holding for $\tau = 1$ h, water cooling
5	Volume HT: heating in BaCl_2 salt bath to $t = 1160^\circ\text{C}$ in $\tau = 1$ min, transfer to salt bath with $t = 380^\circ\text{C}$, holding for $\tau = 1$ h, water cooling
6	Volume HT: heating in BaCl_2 salt bath to $t = 1160^\circ\text{C}$ in $\tau = 1$ min, oil cooling

different phases at a temperature lower than the melting temperatures of the individual substances corresponding to these phases. Contact melting begins at an almost eutectic temperature, and a liquid phase can appear in the contact zone upon very rapid heating at temperatures below the equilibrium eutectic point in the systems where intermetallics can form [16].

The purpose of this work is to study the structure and the properties of the transition layer in HSSGCI castings with the surface melted upon heat treatment. Graphite globules in this layer are coated with a ledeburite shell. We also formed such a structure in macrovolumes to use its advantages to increase the reliability of the machine components operating under abrasive wear and high contact and dynamic loads.

EXPERIMENTAL

We studied VCh50 cast iron samples with spheroidal graphite, which were cut off from experimental ingots with a wall thickness of 24 mm cast into a dry sand–clay mold. Table 1 gives the chemical composition and the mechanical properties of the cast iron samples.

The microstructure of the ingots consisted of a pearlitic–ferritic metallic base with spheroidal graphite inclusions. Ferrite was located around the graphite inclusions and its content did not exceed 30%.

The chill layer at the VCh50 cast iron sample surfaces was formed by LHT with surface melting and by RF current quenching with surface melting.

Heating during volume heat treatment (HT) was performed in a barium salt bath. Cooling was carried out according to the following two schedules: continuous and isothermal quenching. Table 2 presents the general characteristics of HT used to form the given properties of cast iron. At the end of volume HT, we performed tempering at $t = 260^\circ\text{C}$ for $\tau = 2$ h.

The microstructures of the samples were analyzed with a Neophot-21 optical microscope on polished sections etched by 4% nital. The hardnesses of the phases and structural constituents of cast iron were determined using a PMT-3 device. The total hardness, strength, and impact toughness were estimated by standard test methods according to GOSTs 9012–59, 9013–59, 1497–84, 9454–78, and 9450–76.

The abrasive wear resistance of cast iron samples with different structures was determined by comparative tests performed on an end-face device with fixed abrasive. Carborundum with a grain size of 100–125 μm was used as the abrasive counterbody.

The wear of the samples was determined from the sample mass decrement in the same time intervals during tests. For a comparative estimation of the wear resistances of various materials, we used the relative wear resistance

$$\varepsilon_i = \Delta m_i / \Delta m_{st},$$

where Δm_i and Δm_{st} are the sample i and standard mass losses, respectively, under the same wear conditions. The standard was normalized grade 45 steel.

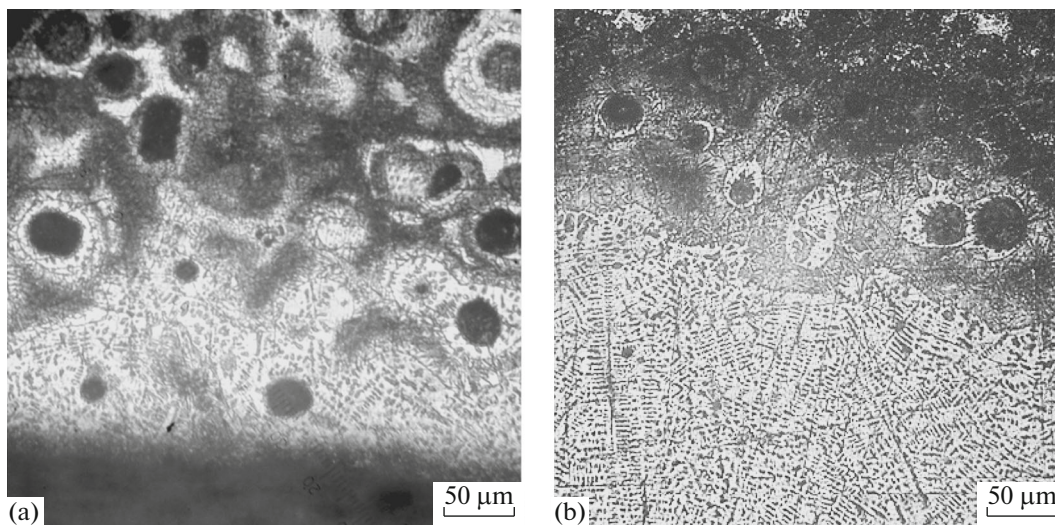


Fig. 2. Micrographs of the chill and transition layers in the VCh50 cast iron samples subjected to surface melting during HT: (a) laser HT ($\times 250$) and (b) RF current HT ($\times 250$).

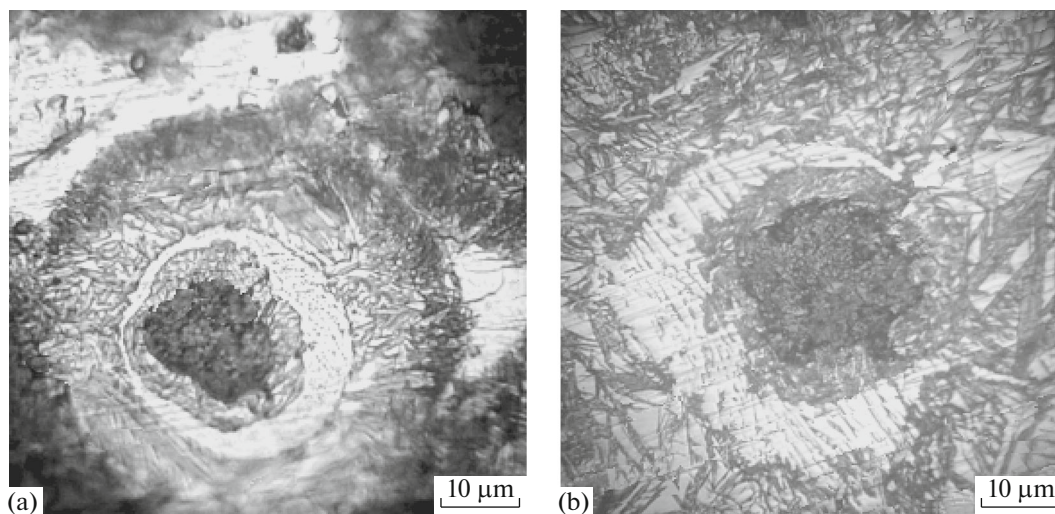


Fig. 3. Micrographs of the multilayer shells around graphite inclusions in VCh50 cast iron, which formed during (a) laser ($\times 800$) and (b) RF current quenching ($\times 800$).

RESULTS AND DISCUSSION

A thin transition layer, where only contact melting at the graphite/metallic base interface takes place, forms in the microstructure of the spheroidal graphite cast iron after laser and RF current quenching with surface melting. This layer is adjacent to the zone subjected to complete melting at the stage of heating and having a ledeburite structure after HT. The molten metal solidified at a high supercooling and ledeburite formed due to intense heat removal to the cold sample volume (Fig. 2).

The thickness of the chill layer with a ledeburite structure in the LHT-quenched sample is 0.12 mm, and the transition layer thickness is 0.095 mm. In the sample after RF current quenching, these parameters are 0.90 and 0.084 mm, respectively.

Multilayer shells form around graphite inclusions as a result of contact melting, graphite dissolution, intense diffusion saturation of the metallic base by carbon, and subsequent fast cooling (Fig. 3).

The inner layer of the shell after laser quenching consists of fine acicular martensite and a ledeburite layer is then located. The next layers are as follows:

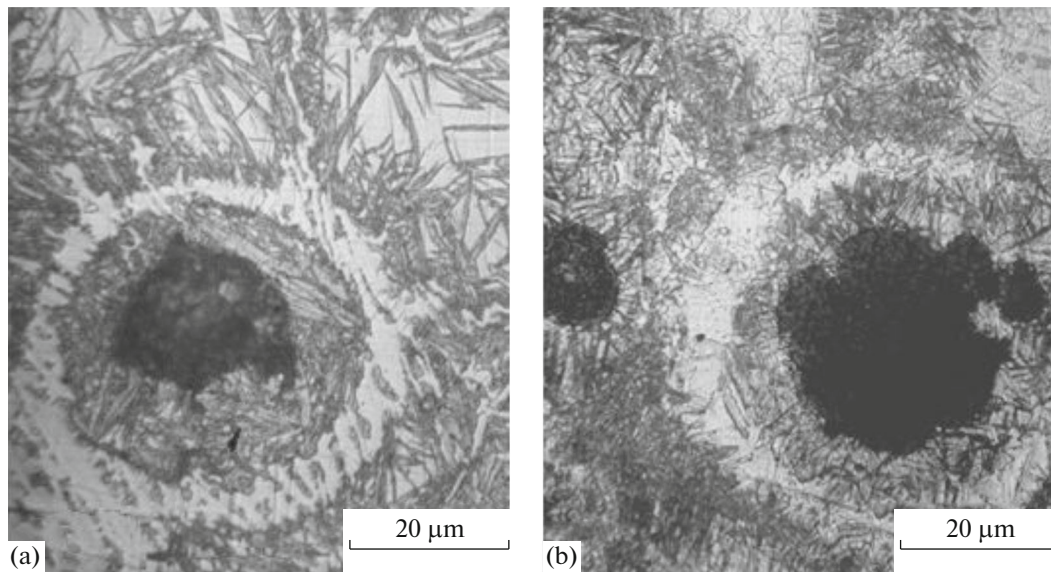


Fig. 4. Micrographs of the two-layer shells around the graphite inclusions in VCh50 cast iron after (a) continuous ($\times 700$) and (b) isothermal ($\times 1000$) quenching from 1160°C .

austenitic–martensitic layer with coarse needles, martensitic layer, troostite layer, and a layer of the ferritic shell retained from the initial structure. The metallic matrix is mainly represented by troostite and martensite. After RF current quenching, the shells around graphite inclusions only have the first two layers, and the metallic base consists of austenite and martensite.

The general schedule of volume HT for the formation of a ledeburite shell around graphite globules was based on an analysis of the available data on the conditions of formation of such structures in the transition zone in the cast iron quenched by LHT or RF current with surface melting and our preliminary experimental results. This schedule included fast heating of the cast iron samples to the eutectic temperature in the salt BaCl_2 melt. The melting temperature ($^{\circ}\text{C}$) of the eutectic in the cast iron under study was calculated using the following formula from [17], where the influence of the cast iron components was studied: $t_e = 1153 + 4[\text{Si}] - 2[\text{Mn}] - 30[\text{P}] = 1153 + 4 \times 2.71 - 2 \times 0.51 - 30 \times 0.1 = 1159.82^{\circ}\text{C}$.

The time of holding the samples in the salt bath at $t = 1160^{\circ}\text{C}$ was chosen to heat them to this temperature at a depth of at least 15 mm and to melt a thin layer at the austenite/graphite interface without melting of the eutectic throughout the metal volume. The best result was achieved at a holding time $\tau = 1$ min. The deceleration of the heating rate during 10-min holding at $t = 850^{\circ}\text{C}$ suppressed contact melting: a liquid phase appeared along eutectic cell boundaries rather than at the graphite/metallic base interface.

Cooling of the samples from $t = 1160^{\circ}\text{C}$ was carried out during continuous oil quenching. Isothermal

quenching was performed in a saltpeter bath at $t = 380^{\circ}\text{C}$ on holding for $\tau = 1$ h, and the samples were then water cooled. As a result of this treatment, a microstructure with graphite inclusions surrounded by a shell consisting of martensite, ledeburite, and bainite layers forms throughout 24×24 -mm VCh50 cast iron samples (Fig. 4).

The metallic base of the samples subjected to continuous quenching has the structure of coarse acicular martensite and austenite in an amount up to 40%. After isothermal quenching, the structure consists of bainite and austenite.

The microhardnesses of the shells around graphite inclusions are as follows: the ledeburite layer has a microhardness of 9200–9900 MPa; the martensitic–austenitic layer, 6300–6700 MPa, and the troostite–martensite layer, 3300–3600 MPa.

After volume isothermal quenching from 950°C according to schedule 4 (Table 2), the microstructure of cast iron consists of ausferrite and graphite inclusions.

Figure 5 and Table 3 present the results of wear resistance tests and the mechanical properties of the VCh50 cast iron with different structures of the metallic base and the high-carbon component.

The comparative tests demonstrate that the cast iron samples with the chill surface layer formed upon laser or RF current quenching have the maximum wear resistance. However, the chill layer has been worn in a short time and the wear intensity of the samples increases rapidly and approaches the level of the untreated metal. For many rapidly worn parts, the formation of a chill layer, the thickness of which is com-

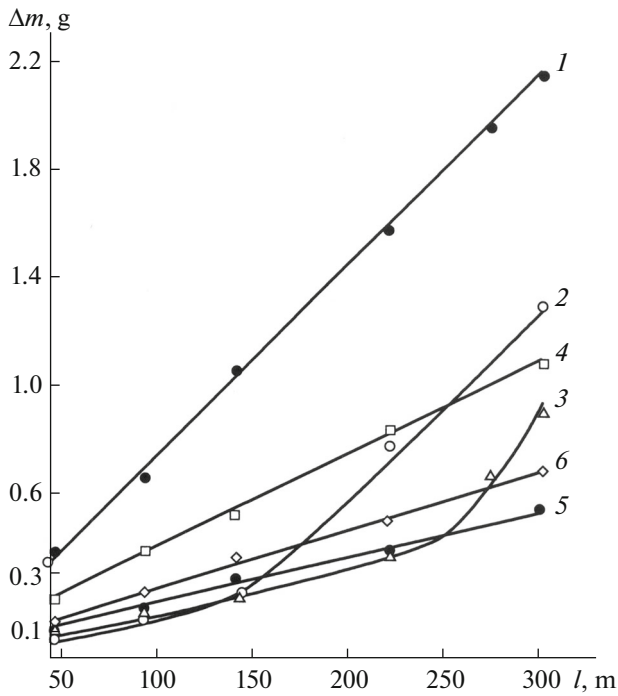


Fig. 5. Wear dynamics of the samples subjected to abrasive wear resistance tests (l is the friction path length): (1) grade 45 steel, normalizing (standard for comparison); (2) VCh50 cast iron, laser quenching with melting; (3) VCh50 cast iron, RF current quenching with melting; (4) VCh50 cast iron, volume isothermal quenching; (5) VCh50 cast iron, contact melting, isothermal quenching at $t = 380^\circ\text{C}$; and (6) VCh50 cast iron, contact melting, oil quenching.

comparable with the allowable wear thickness, during HT is restricted by the possibilities of modern equipment.

The HSSGCI samples after volume HT according to schedules 5 and 6 have the best set of properties, which determines a high operate reliability of products. The precipitation-hardened structure that meets Charpy's principle formed in the samples after HT according to these schedules. The formation of hard

shells around graphite inclusions in the cast iron with an ausferrite metallic base almost doubled its wear resistance at a high retained level of strength and impact toughness. Continuous quenching-induced cooling (schedule 6) for the formation of a martensitic–austenitic structure in the metallic base slightly increased the wear resistance, and the impact toughness decreased. However, it exceeded its value in the initial as-cast state of the cast iron due to a high content of retained austenite.

An important advantage of volume HT, when only contact melting takes place, is the absence of surface casting defects (blowholes, surrounding roughness), which form after complete melting of a surface layer.

The hardness of the ledeburite shells of graphite inclusions is significantly higher than those of the bainite and martensite shells in the hard eye structure. Therefore, the formation of ledeburite shells around graphite globules enhances their efficiency as reinforcing particles and opens up fresh opportunities for improving the properties of cast iron due to the use of a ferritic or pearlitic–ferritic matrix and a wide spectrum of structures, including ausferrite, bainite, and martensite + austenite. As a result, the field of application of materials with a hard eye structure for the production of products, the service requirements of which include strength characteristics, high wear resistance, and brittle fracture resistance, is significantly widened.

CONCLUSIONS

(1) The microstructure of HSSGCI, which consists of an ausferrite metallic matrix and uniformly distributed graphite globules coated with a shell of martensite and ledeburite layers, ensures high wear resistance, strength, and impact toughness of as-cast products according to Charpy's principle of producing precipitation-hardened composites.

(2) This structure of HSSGCI can be formed by volume HT, which consists of rapid heating to the

Table 3. Mechanical properties and wear resistance of the VCh50 cast iron samples subjected to HT according to schedules 2–6 (see Table 2)

HT schedule	Mechanical properties			ε_i
	σ_u , MPa	KC , J/cm ²	H_{50} , MPa (total HB)	
2	610	12.5	Surface—10210 ± 1403; (total—238)	Chill layer—5.0, then to 1.6
3	610	12.5	Surface—10012 ± 1723; (total—238)	Chill layer—4.46, then ≤2.31
4	1380	91.0	(525)	2.03
5	1410	87.3	(510)	3.70
6	1367	17.0	(620)	4.00

eutectic transformation temperature, holding for $\tau = 1$ min, isothermal quenching at $t = 380^\circ\text{C}$ for $\tau = 1$ h, water cooling, and tempering at $t = 260^\circ\text{C}$.

FUNDING

This work was supported by the Ministry of Education and Science of the Russian Federation, grant MD-1125.2017.8 of the President of the Russian Federation.

REFERENCES

1. A. E. Novikov, V. A. Motorin, M. I. Lamskova, and M. I. Filimonov, "Composition and tribological properties of hardened cutting blades of tillage machines under abrasive deterioration," *J. Frict. Wear* **39** (2), 158–163 (2018).
2. V. I. Pyndak and A. E. Novikov, "Tribotechnical and energy assessment of parts of working members of cultivating machines after carburizing and laser hardening," *Metal Sci. Heat Treat.* **58** (3–4), 226–230 (2016).
3. V. S. Doroshenko and V. A. Gnatush, "World market of casting spheroidal graphite iron. State of the art and prospects of development," *Vestn. Armaturostroitel'ya*, No. 5, 112–119 (2017).
4. G. I. Sil'man, K. V. Makarenko, and E. A. Zentsova, "Bainitic high-strength spheroidal graphite cast iron," *Metalloved. Term. Obrab. Met.*, No. 4, 3–8 (2013).
5. V. G. Efremenko, K. Shimidzu, T. V. Pastukhova, Yu. G. Chabak, K. Kusumoto, and A. V. Efremenko, "Effect of volume and surface-plasma heat treatment on the microstructure and erosion wear resistance of complex cast iron with spheroidal vanadium carbides," *Trenie Iznos* **38** (1), 24–31 (2017).
6. Y. Ch. Peng, H. J. Jin, J. H. Liu, and G. L. Li, "Influence of cooling rate on the microstructure and properties of a new wear resistant carbidic austempered ductile iron (CADI)," *Mater. Charact.* **72**, 53–58 (2012).
7. J. Liu, G. Li, X. Zhao, and J. Zhang, "Effect of austempering temperature on microstructure and properties of carbidic austempered ductile iron," *Advanc. Mater. Res.* **284–286**, 1085–1088 (2011).
8. K. V. Makarenko, "Manufacture of mottled cast iron with an ausferritic structure from an as-cast state," *Liteinoe Proizvod.*, No. 2, 2–6 (2010).
9. S. A. Patil, S. U. Pathak, and Ajay Likhite, "Development and wear analysis of carbidic austempered ductile iron (CADI)," *Int. J. Innovat. Res. Sci., Eng. Technol.* **3** (2), 9652–9657 (2014).
10. G. Francucci, J. Sikora, and R. Dommarco, "Abrasion resistance of ductile iron austempered by the two-step process," *Mater. Sci. Eng.* **485** (1–2), 46–54 (2008).
11. K. Okabayashi, M. Kawamoto, A. Ikegana, and M. Tsujikawa, "Impact characteristics of and fractography of spheroidal graphite cast iron and graphite steel with "hard eye structure," *Trans. Jap. Found. Soc.* **1**, 37–41 (1982).
12. K. V. Makarenko and A. A. Poltorukho, "Methods for creating structural shells around the graphite inclusions in high-strength cast iron," *Vestn. Bryansk. Gos. Tekhn. Univ.*, No. 2(38), 64–68 (2013).
13. M. Mett'yuz and R. Rollings, *Composite Materials. Mechanics and Technology* (Tekhnosfera, Moscow, 2004).
14. V. S. Maiorov, "Laser hardening of metals," in *Laser Technologies of Material Treatment: Modern Problems of Fundamental Studies and Applied Development*, Ed. by V. Ya. Panchenko (Fizmatlit, Moscow, 2009).
15. A. V. Makarov, I. Yu. Malygina, and A. L. Osintseva, "Effect of laser treatment on the structure, wear resistance, and fatigue properties of high-strength cast iron," *Fiz. Khim. Obrab. Mater.*, No. 4, 46–55 (2006).
16. A. A. Akhkubekov, S. N. Akhkubekova, A. M. Bagov, M.-A. A. Zubkhadzhev, and Zh. M. Mamaeva, "On the decrease in the contact melting temperature in metallic systems with intermetallics," *Izv. Ross. Akad. Nauk, Ser. Fiz.* **69** (5), 681–685 (2010).
17. *Handbook of Iron Casting*, Ed. by N. G. Girshovich, 3rd ed. (Mashinostroenie, Leningrad, 1978).

Translated by K. Shakhlevich